THE UNIVERSITY OF CHICAGO

A CESIUM-133 EFFUSIVE OVEN FOR ULTRACOLD ATOMIC EXPERIMENTS

A DISSERTATION SUBMITTED TO
THE FACULTY OF THE DIVISION OF THE PHYSICAL SCIENCES
IN CANDIDACY FOR THE DEGREE OF
BACHELOR OF ARTS IN PHYSICS WITH HONORS

DEPARTMENT OF PHYSICS

BY

DYLAN O. SABULSKY

CHICAGO, ILLINOIS

JUNE 2014

Главное, делайте всё с увлечением, это страшно украшает жизнь.
It is important to do everything with enthusiasm, it embellishes life enormously.

Lev Davidovich Landau
(1908-1968)

ACKNOWLEDGMENTS

I would like to thank Cheng Chin (Supreme Leader, advisor, professor and professional physicist) for allowing me into his group, trusting me with incredible projects and allowing me to contribute meaningfully to his laboratory. I have learned so much from him and his group. Cheng's tireless effort and boundless knowledge are inspiring and supportive. His group is made superior by his addition as the leader. Working with him has been one of my greatest and most sincere pleasures.

I want to thank Colin V. Parker for his dedicated help and continued advice on previous and current projects. If I ever win that Nobel Prize (we know I won't but still...), I'll give you that shout-out on stage like I promised! Thanks to Prof. Eric L. Hazlett, the coadvisor for my thesis, for supporting me in the project presented here, giving well thought out advice, and for looking out for me and checking in despite having so much to do. I know you will be an incredible professor for the students at Carleton College! My sincere thanks to Karina Jiménez-García for helping me during the editing process and supporting me throughout the writing process.

I would love to thank Paloma L. Ocola, my incredible assistant, and the graduate students Lei Feng, Gustaf Downs and Li-Chung Ha for their assistance, effort, friendship, and advice. I also wish to thank Logan Clark, Jacob Johansen and Shih-Kuang Tung for insightful conversation and Helmut Krebs for machining advice. I need to thank the venerable Prof. Philippe Guyot-Sionnest for helping us placing the ^{133}Cs ingot into the oven; we definitely would have broken a few things, blown up a few more things, maybe hurt ourselves and caused a building lockdown if not for his steady hand...

My parents, Barbara Banahene-Gibbs and Scott Neil Sabulsky, deserve a few words for their support. I have found them to be an incredible resource for life advice; despite not understanding what I study or why, they have proven time and again that they will be there for me.

Last, I would like to thank the undergraduate physics advisor, Stuart Gazes, for all his support. You are a legendary physics teacher. Thank you for bringing our passion to many young students while touching and changing the lives of people in the major. You make the department shine along with Van Bistrow and Mark Chantell, the cantankerous laboratory supervisors.

The James Franck Institute has been my home for almost four years now. It is an exciting and intense collaborative environment. The people that inhabit it make all the hard work fun; all the events we host always serve to brighten and broaden my perspective. I hope more undergraduate students find their way into the JFI and come to love it as much as I do.

The author acknowledge support from the NSF-MRSEC program, the NSF Physics REU program, NSF Award No. PHY-1206095, AFOSR-MURI, and ARO-MURI 63834-PH-MUR. This honors thesis was refereed by Prof. Kathryn Levin, Prof. Yah Wah, Prof. David Reid and Prof. Stuart Gazes of the Department of Physics, The University of Chicago. The author declares no competing financial interests.

ABSTRACT

We present the design, construction and characterization of a high-flux ^{133}Cs effusive oven for experimental research on many-body phenomena with ultracold Cs atoms. The oven is constructed of readily available UHV components and requires minimal machining. The atomic sample, a 5 g ingot of ^{133}Cs, is contained inside a Pyrex ampule reservoir and is electrically heated to the desired temperature. An integrated all-metal valve isolates the main experimental chamber from the oven, simplifying the oven reload process. Our oven design includes graphite briquettes acting as a ^{133}Cs getter; this helps to improve our ultra high vacuum as well as to protect our ion pumps. The coldfinger includes two thermoelectric coolers, ensuring atomic beam collimation with minor divergence, $(\alpha)_{1/e} = 1.7°$, before the Zeeman slower. A bright wall collimation scheme allows us to produce a well collimated ^{133}Cs atomic beam with a measured flux of 8.14×10^9 $\frac{\text{atoms}}{\text{s}}$ at 90 °C. We report on the velocity distribution of atoms in the beam and the width of the beam at an oven temperature of 90 °C and valve temperature of 144 °C. This oven design can be readily adapted to other alkali metals with minor modification to the oven heating elements.

LIST OF FIGURES

Part I

Constructing and Characterizing a Cs Effusive Oven

CHAPTER 1

INTRODUCTION

Ultracold atom experiments with samples of ^{133}Cs are well studied in experiments ranging from quantum criticality [1] and universality in 2D Bose gases [2] to effective ferromagnetic domains [3]. All of these experiments are based around an effusive atomic beam oven feeding a well collimated beam into an ultra high vacuum (UHV) (below 10^{-10} torr) region. A reliable, collimated atomic beam is a critical component of cold atom experiments. While there exist many different sources for atomic beams, effusive ovens are simple, robust and can produce a high atomic flux at moderate temperatures depending upon the atomic species. The goal of this project is to construct an effusive atomic oven to quickly and efficiently load into a magneto-optical trap (MOT) while maintaining good UHV and a long operational lifetime.

Here we present a high-flux effusive oven designed for extended-lifetime operation and simple reloading for ultracold atom experiments based on ^{133}Cs. Our oven uses an ampule/collimation scheme designed to conserve the source substance, a bright wall collimator scheme made with an UHV nipple and an efficient external coldfinger to reduce wall reemissions. We introduce a ^{133}Cs gettering material, graphite, to improve the UHV by capturing atoms that are not in the beam and/or reemitted atoms from the collimator walls. Here, we present an oven design for ^{133}Cs that can be generalized as a high-flux atomic beam for other atomic species. Simple modifications to the oven heating element to accommodate different temperatures would be necessary (e.g. like using an all-metal container for the sample) along with a possible substitution of gettering material depending on the source. For a review of atomic sources, see Ross *et al* [4].

CHAPTER 2

EFFUSIVE ATOMIC OVENS

The effusive regime, also known as the molecular flow regime, is characterized by the dominance of atom-wall collisions. This can be expressed through the mean distance along which atoms propagate between two successive collisions, i.e. the mean free path,

$$\lambda = \frac{1}{\pi n d_0^2 \sqrt{2}}, \tag{2.1}$$

where d_0 is the atomic diameter and n is the atomic density. If the mean free path is smaller than the diameter of some aperture d_1, the atoms collide frequently before emerging from the oven. This leads to hydrodynamic flow and collective transport processes. The effusive regime occurs when the mean free path is larger than the aperture diameter,

$$\lambda > d_1. \tag{2.2}$$

2.1 Determining Atomic Flux in the Effusive Regime

The velocity distribution of atoms inside the oven is described by the 3D Maxwell-Boltzmann distribution,

$$P_{\mathrm{v}}(T) = C\left(\frac{m}{k_B T}\right)^{3/2} v^2 \exp\left(-\frac{mv^2}{2k_B T}\right), \tag{2.3}$$

where C is some normalization constant, k_B is Boltzmann's constant, T is temperature in Kelvin, m is the mass of a single atom and v is the velocity. The most probable velocity and the mean velocity are

$$v_{\mathrm{prob}} = \sqrt{\frac{2k_B T}{m}} \quad \text{and} \quad \bar{v} = \frac{2v_{\mathrm{prob}}}{\sqrt{\pi}} = \sqrt{\frac{8k_B T}{\pi m}}, \tag{2.4}$$

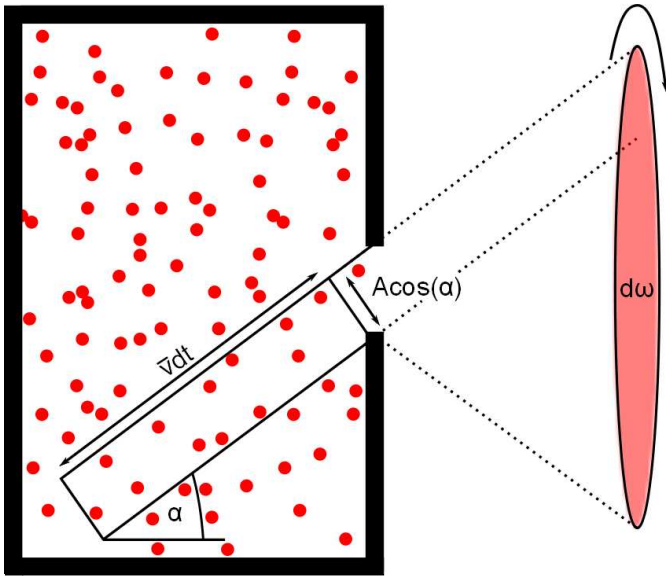

Figure 2.1: Solid angle of an emerging atomic beam. In some time interval, an atomic volume $V = \bar{v}A\cos(\alpha)\mathrm{d}t$ leaves the oven with an angle of emergence α. Adapted from Schindler [5].

respectively. The number of atoms $\mathrm{d}N$ per unit time $\mathrm{d}t$ leaving the oven is given by the unit flux $\mathrm{d}\Theta$, see Fig. 2.2,

$$\mathrm{d}N = \mathrm{d}\Theta\mathrm{d}t = \frac{\mathrm{d}\omega}{4\pi}\bar{v}nA\cos(\alpha)\mathrm{d}t, \tag{2.5}$$

where $A = d_1^2\pi/4$ is the area of the aperture and α is the angle of emergence. Integrating over the solid angles

$$\mathrm{d}\omega = 2\pi\sin(\alpha)\mathrm{d}\alpha \tag{2.6}$$

gives the total atomic flux from the oven,

$$\Theta = \int_0^{\pi/2}\mathrm{d}\omega = \frac{1}{4}\bar{v}nA. \tag{2.7}$$

The Beer-Lambert Law successfully describes the transmission of light with incident intensity I_0 through the atomic beam [6] as

$$I = I_0\exp(-D), \tag{2.8}$$

where D is related to the optical density of the atomic beam, OD by

$$D = \ln(10)OD \approx 2.3OD. \tag{2.9}$$

For small angles α from the beam axis, an atomic beam interacting with a laser beam over the light-atom interaction length j[1], D is defined as

$$D = \int_{x_1}^{x_2} n(x)\sigma_0 \mathrm{d}x \approx n\sigma_0 j, \tag{2.10}$$

where σ_0 is the cross section for the absorption of a resonant photon by an atom [7]. The simple two level system model, appropriate for the D1 transition in ^{133}Cs considered here[2], defines the absorption cross section as

$$\sigma_0 = \frac{14\lambda^2}{25\pi} \approx 1.413 \times 10^{-9}\ \mathrm{cm}^2 \tag{2.11}$$

for resonant light[3] [18]. Combining the above equations yields the atomic density,

$$n = -\frac{25\pi}{14\lambda^2 j} \ln\left(\frac{I}{I_0}\right) \tag{2.12}$$

By measuring I_0, I and j, we can calculate the atomic density, which in turn leads to a calculation of the total flux. out of a source with aperture diameter d_1 and temperature T,

$$\Theta_{\mathrm{tot}} = \frac{25}{112}\frac{\pi^2 d_1^2}{\lambda^2 j} \ln\left(\frac{I_0}{I}\right)\sqrt{\frac{2k_B T}{\pi m}}. \tag{2.13}$$

1. In general, j is not equal to the atomic beam diameter. Atoms that are not in the center have velocity components in the direction of the laser beam, so their resonance frequencies are Doppler shifted. These atoms do not interact with the light.

2. The following calculation is strictly for the D1 transition with randomly polarized light.

3. For the D1 transition, the effective resonant cross-section with randomly polarized light; there is polarization dependence in the Clebsch-Gordon coefficient.

Only atoms leaving the oven at small angles are useful for experimentation; these atoms travel through the beam assembly without wall collisions, directly into the Zeeman slower. It becomes necessary to block a large fraction of the atoms that have a sufficiently large angle of emergence; these atoms do not contribute to the atomic beam and go on to deposit on the walls of the apparatus, causing subsequent problems when reemitted from the wall such as raised pressure and decreased experiment quality.

We chose to pursue an efficient bright wall collimator oven design aiming to minimize the waste of source material as well as to prevent the eventual failure of the collimation stage and the release of source material in unwanted directions. Various techniques exist to decrease loss from poorly collimated source material; these techniques can be divided into three types: (i) dark wall collimators, (ii) bright wall collimators and (iii) recirculation ovens.

Dark wall collimators use geometric shadowing to cut off source emission in unwanted directions. This is satisfactory for incredibly intense and short operational periods, but is problematic for elements like ^{133}Cs. A dark wall collimator using a graphite collimator to absorb impacting Cs atoms will soon saturate; the subsequent reemission of atoms can potentially alter the geometry of the collimator, therefore ruining the beam shape [8].

Bright wall sources, or sources where the wall is hot, avoid the saturation problems of the dark wall collimator but provide less effective collimation due to atoms reemitting from walls of the collimation tube. Neither bright or dark wall sources take advantage of source material that is wrongly directed; this is a reason to consider a recirculating oven[4]. Wall reemissions and wrongly directed source material can be suppressed in bright wall collimation schemes. By reducing the temperature of the walls of the collimator to make source material stick upon first impact. Furthermore, by constructing a collimation scheme with appropriate UHV components to ensure the source can be reloaded without venting the whole oven assembly to atmosphere, bright wall collimators make efficient atomic beam collimators for

4. Recirculating oven sources work by capillary action of a steel mesh or porous wicking walls to return material to the source [9, 10]; however they are complicated to produce and operate.

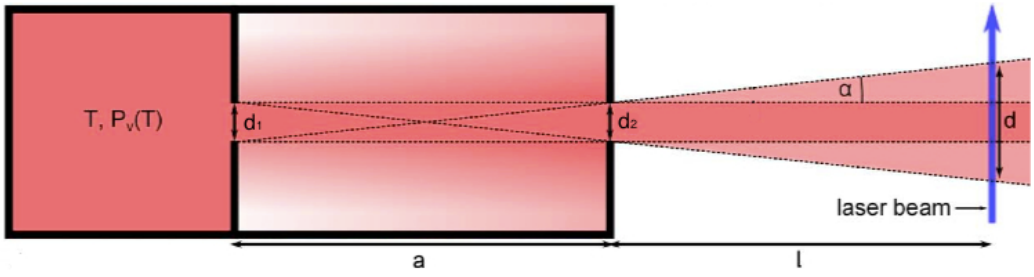

Figure 2.2: Bright wall collimator effusive oven scheme. Only atoms within the dotted lines contribute to the atomic beam leaving the oven. For our oven design, $d_1 = d_2$. Adapted from Schindler [5].

long term use.

Recirculating oven sources are complicated to produce and operate. Wall reemissions and wrongly directed source material can be suppressed in bright wall collimation schemes. By reducing the temperature of the walls of the collimator to make source material stick upon first impact and by constructing a collimation scheme with appropriate UHV components to ensure the source can be reloaded without venting the whole oven assembly to atmosphere, bright wall collimators make efficient atomic beam collimators for long term use.

It is a common technique in ultracold atom experiment is to use bright wall collimators, see Fig. 2.2, while heating the apertures to prevent blockages; this conserves source material and extends the source lifetime. Provided that the mean free path of the atoms is larger than the geometry of the oven, one can neglect that the apertures are heated and continue on to the following approximation. The atomic beam emerges into a solid angle ω around the propagation axis (down the beam assembly toward the Zeeman slower) described by

$$\omega = 2\pi\left[1 - \cos\left(\tan^{-1}\left(\frac{d_1}{a}\right)\right)\right], \tag{2.14}$$

where a is the distance between apertures. Note, we use two apertures of the same diameter d_1. The collimation ratio is $f = \frac{d_1}{a}$. At some distance ℓ from the second aperture, the beam

diameter is

$$d = 2\left(d_1 a(a+\ell) - \frac{d_1}{2}\right). \tag{2.15}$$

The flux through the aperture is obtained by integrating over the bounds of interest,

$$\Theta(d_1) = \int_0^{\tan^{-1}|f|} \mathrm{d}\omega = \frac{1}{4}\bar{v}nA\frac{f^2}{1+f^2}, \tag{2.16}$$

which gives the atomic flux injected into a certain angle around the beam axis.

2.2 ^{133}Cs Gettering with Graphite

A gettering material is one that is placed inside of a vacuum system for the purpose of completing and maintaining vacuum. When gaseous atoms impact upon the getter material, they either combine chemically or undergo absorption. This technique is commonly used in atomic clocks on satellites in geosynchronous orbit to increase the operational lifetime of the satellites. Graphite and antimony are both known to be good ^{133}Cs gettering materials. Graphite can hold up to 20% of its mass in absorbed ^{133}Cs and is far easier to use and handle than antimony [11]. We use graphite as a non-evaporable bulk (NEG) getter for ^{133}Cs. The gettering of ^{133}Cs with graphite can be characterized through measurements of the sticking coefficient of ^{133}Cs on graphite [14]. This measurement is taken relative to a paraffin coated surface, known to be perfectly nonsticking [15]. The sticking coefficient γ is defined as

$$\gamma(\theta) = 1 - \frac{\theta_g}{\theta_p} \tag{2.17}$$

where θ_g is the reflected signal from the graphite at angle θ and θ_p is the reflected signal from paraffin at the same angle θ [16], see Fig. 2.3.

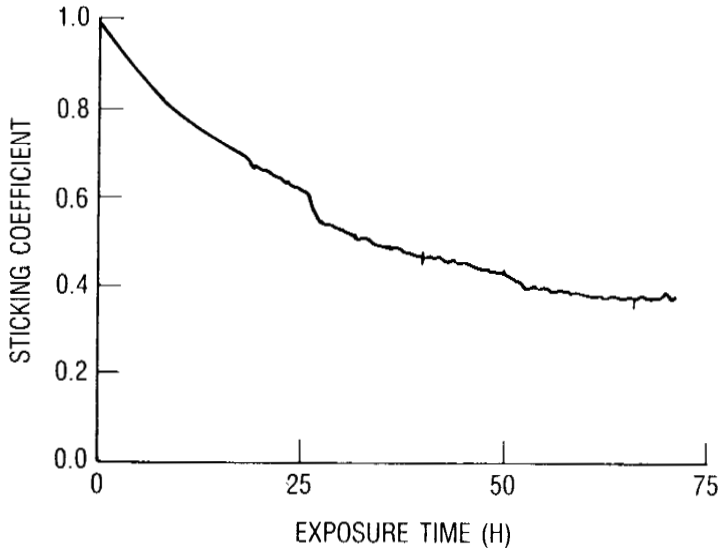

Figure 2.3: The decline of the sticking coefficient γ with exposure time for ^{133}Cs gettering with graphite. Experimental data adapted from Bashkar *et al* [11]. The ^{133}Cs beam flux incident on the graphite sample was 6.2×10^{11} atoms s^{-1} cm^{-2}.

CHAPTER 3

OVEN DESIGN

3.1 Introduction

Designing an atomic source for an ultracold atom experiment is in principle a straightforward task, specially due to the ease with which alkali metals can be made to reach a sufficiently high vapor pressure. For instance, ^{133}Cs melts at a mere 28.55 °C and can reach a vapor pressure of 3×10^{-4} torr at 90 °C. We load our oven with a 99.95% pure ^{133}Cs from Sigma-Aldrich[1].

In summary, the atomic source consists of: (i) a Pyrex reservoir filled with a 5 g ingot of ^{133}Cs ; (ii) a fiberglass heater tape acting as the resistive heating element; (iii) an all-metal angle valve connecting the reservoir the system; and (iv) a bright wall collimator consisting of a pair of copper gaskets with 2 mm apertures each, held by a nipple thermally coupled to an external copper coldfinger. A cube is attached immediately after the collimator to implement a transverse laser cooling scheme.

The following sections are dedicated to the detailed description of the constituents of the oven and techniques used to characterize the atomic source. The whole design is shown in Fig. 3.1 and a table of components is compiled in appendix A.

3.2 Coldfinger Operational Characteristics

The coldfinger contains two thermoelectric coolers and is water cooled, see Fig. 3.2 and appendix B. This allows the walls of the nipple to be cold while the bright wall collimator apertures can remain warm enough to prevent blockage. We need the walls of the nipple to be cold to allow ^{133}Cs to stick to the wall; this reduces the number of atoms that leave the collimator at sub-optimal capture angles.

1. Sigma-Aldrich Website

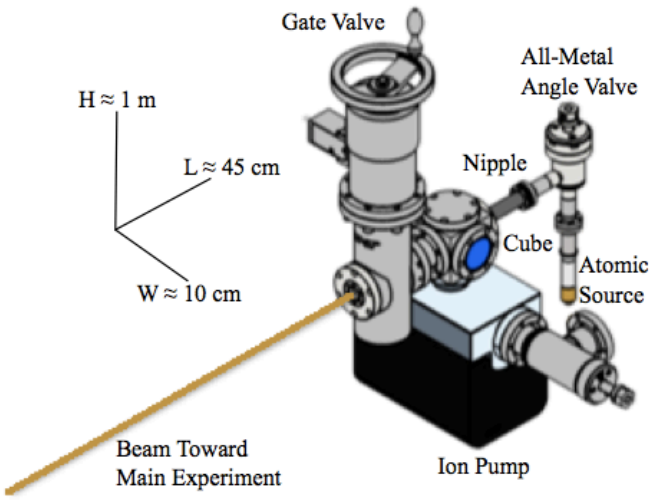

Figure 3.1: High-flux ^{133}Cs effusive oven. The gold line indicates the collimated beam of ^{133}Cs exiting the oven; this beam would then enter the Zeeman slower. Compiled in Autodesk Inventor under educational license. All part designs obtained from their respective manufacturers.

The vapor pressure of the atomic species sets the desirable temperature for the bright wall collimator. Once this information is known, the appropriate thermoelectric cooler (TEC) can be chosen, based on maximum temperature difference and required wattage. For our ^{133}Cs oven bright wall collimator we require that the nipple be kept below 0 °C. We use two potted TECs (TE Technology, TE-127-1.0-2.5, potted with epoxy) above and below the coldfinger. With the apertures kept at 50 °C and minimal insulation the coldfinger was able to maintain temperatures below -3 °C. Heat is dissipated from the TECs with cooled water at a rate of 3.8 liters/min. When mounted, the coldfinger is housed in a combined insulating jacket of styrofoam and polystyrene, allowing even lower temperatures.

3.3 The UHV Cube and All-Metal Gate Valve

The cube has six available connections allocated as follows: (1) leads to the oven assembly, (2) connects to the ion pump, (3) connects to the gate valve and subsequently to the main experiment through the Zeeman slower, (4) is sealed with a blank containing blind taps, and

(5-6) lead to uncoated glass windows, see Fig. 3.1.

The connection to the ion pump contains a customized copper gasket that holds a graphite crucible in; the graphite crucible has its bottom blown out to form a tapered cylinder. This has a significant surface area for the ^{133}Cs to impact upon while being drawn toward the ion pump. We project that this will improve the ion pump lifetime given that Cs can potentially destroy the electrodes in the ion pump over time. All machining was accomplished without specialized tools or machines; the graphite was easily machined in a lathe at low to medium speeds.

The cube connection that leads to the main experiment is attached to a reducer which feeds into the Zeeman slower. The blank with blind tapped holes on the UHV side has a vacuum screw in it to secure a disk of graphite to the UHV side; this captures ^{133}Cs atoms that stray from the beam and ricochet off the sides of the cube.

There are two safety measures in the oven system to prevent ^{133}Cs from collecting in the science chamber, should immediate shut down be necessary. First is the all-metal valve connected to the oven; this can be manually closed to block the gas from reaching the bright wall collimator. Second is the high performance all-metal gate valve; this device can be manually and electrically closed. We chose not to use a wobble stick because of its potential inefficiency to stop the flow into the science chamber; the atomic beam tails could be missed entirely by the wobble stick. Further, impacting atoms can bounce off the wobble stick, impact upon the walls of the oven and reemit, and eventually find their way into the science chamber. Due to these concerns, we decided to use a heavy duty gate valve and a reliable all-metal valve.

3.4 Creating and Maintaining UHV

Modern ultracold atom experiments maintain UHV on the order of 10^{-10} torr to 10^{-13} torr in order to minimize the chance of stray atoms with large kinetic energies colliding with

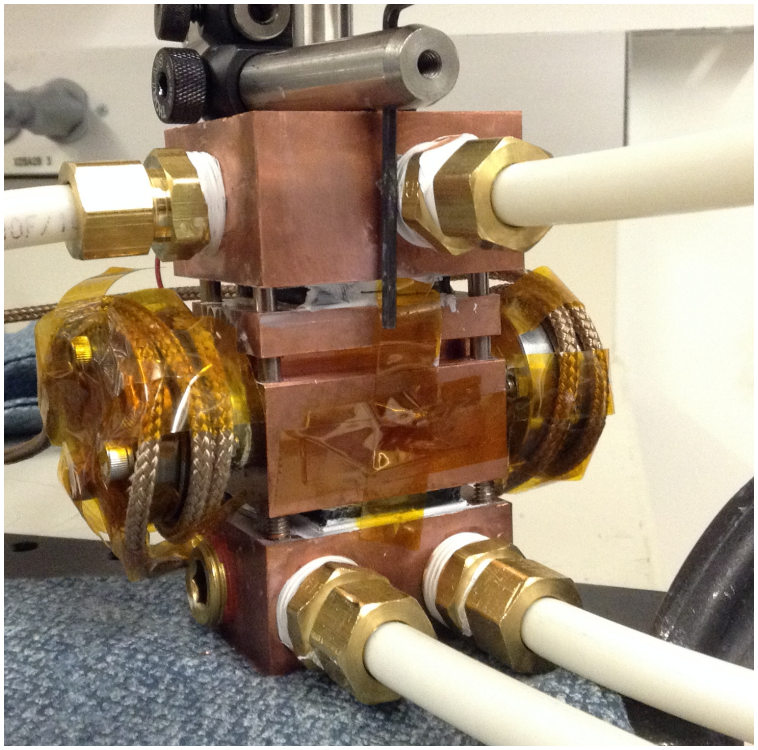

Figure 3.2: Nipple coldfinger. We have developed a coldfinger to prevent ^{133}Cs from leaving the bright wall collimator at sub-optimal angles of emergence. We accomplish this by using a combination of water cooling and thermoelectric cooling to keep the neck of the nipple below -3 °C against standard room temperature and pressure. The collimating copper gaskets are kept between 40 and 50°C to prevent Cs from condensing in the aperture. The top and bottom copper pieces are water cooled. Between the water cooled copper pieces and the copper clamps holding the nipple are the thermoelectric coolers. Thermal paste was used to optimize thermal coupling.

atoms in the main trap. Creating and maintaining UHV in cold atom experiments takes standard vacuum techniques [17]. Using metal gaskets allow for evacuating the system at high temperatures; elastomer gaskets can not withstand the high temperatures commonly used to clean vacuum parts. An ion pump constantly pumping our oven (40 liters/second) is required to maintain UHV.

Elevating the temperature of a vacuum system increases the outgassing rate; outgassing is the process that determines the final pressure of the system. Heating the system during evacuation accelerates the removal of gas from the system. This technique for reaching UHV is commonly called “baking”. In our application, we are removing mostly water and

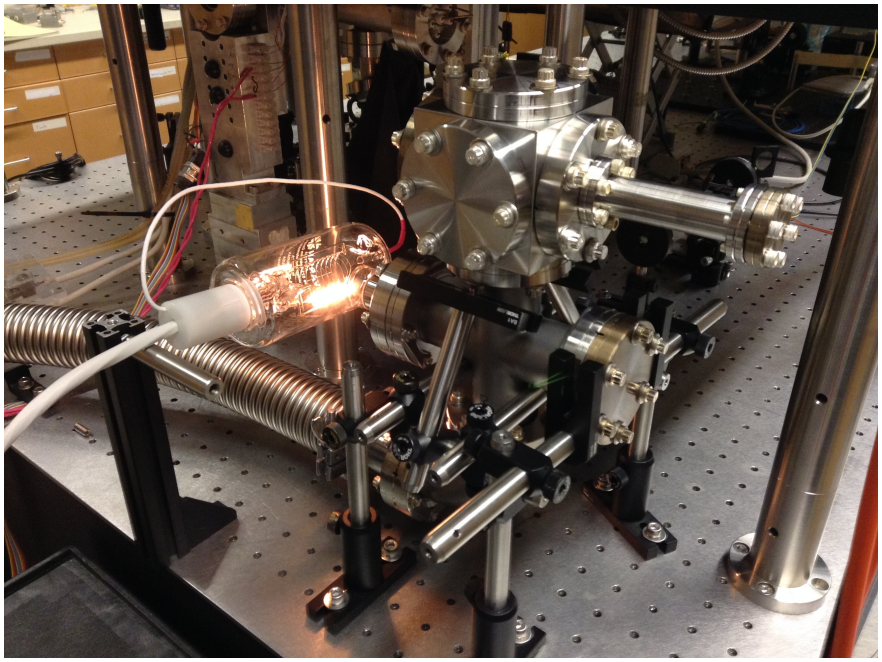

Figure 3.3: High temperature bake scaffold and extended graphite baking. The scaffold is constructed out of optical posts and mounts. We use an elbow to connect the turbo pump to the cross. The connection of the cross lead to the turbo-pump, the cube, a blank and a Varian 571 Ion Gauge. We added thermocouples to the bellows, the cross and the cube. After covering the three main components in fiberglass heater tape and aluminum foil we started the bake. We reached a maximum cube temperature of 405 °C, cross temperature of 277 °C and bellows temperature of 125 °C. The bright filament shown in the figure is an ion gauge used to monitor the pressure.

hydrocarbons from fingerprints and machining activities [17].

Graphite is a porous material that can trap water, hydrocarbons and other chemicals. We decided to bake the components containing graphite for an extended period of time prior to the final oven construction in order to make the graphite vacuum compatible. We baked and pumped the cube containing the graphite components between 393 °C and 405 °C until we reached a pressure of 3×10^{-8} torr, see Fig. 3.3 and 3.4. To achieve these temperatures we covered the sealed components in fiberglass heater tape connected to variable autotransformers (variacs). We then add on five layers of aluminum foil, reflective side down, to trap air layers for insulation and achieve uniform heating.

After final construction we baked the whole assembly at 180 °C for an additional 2 weeks.

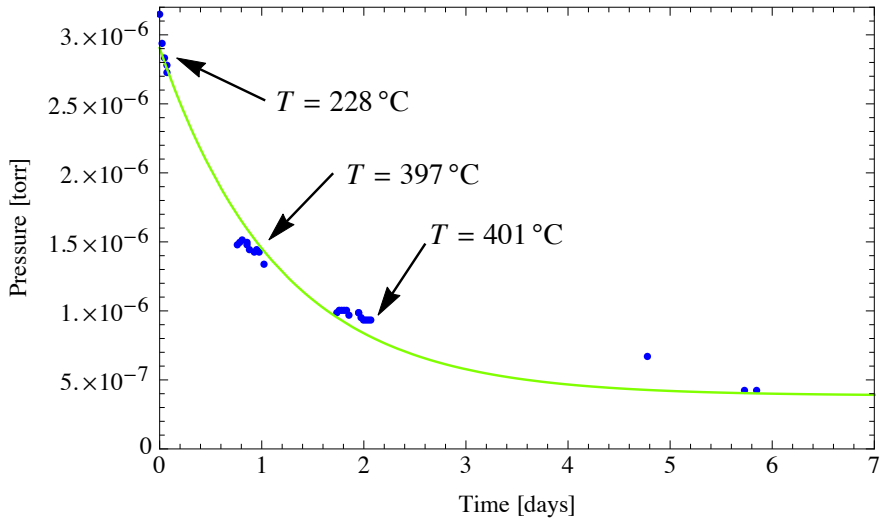

Figure 3.4: High temperature bake vacuum measurements over one week. High surface temperature of the steel transfers kinetic energy to molecules trapped on the surface. These molecules gas off and are brought out of the system via the turbo pump and ion pump. Over 5.4 weeks of baking we saw the pressure drop exponentially from 10^{-5} torr to 10^{-8} torr without using the ion pump. HV is generally regarded as 10^{-8} torr and UHV is considered 10^{-9} torr or lower.

We used a significantly lower temperature for this second bake due to the lower temperature tolerance of the glass to metal transition on the windows. If heated too quickly or too high, thermal mismatch can destroy the window which would vent the oven to atmosphere; we heated the windows by adding copper cups over them the evenly distribute heat and raise the temperature at a rate of 20-25 °C/hr. Further, the ion pump is sensitive to extreme heat unless the magnets are removed.

CHAPTER 4

OPERATIONAL CHARACTERISTICS OF THE ATOMIC BEAM

4.1 Measuring the Beam Width

Integrating an atomic oven system into our larger experimental setup involves characterizing the atomic beam in order to aim it toward the Zeeman slower and the capture area of the MOT. To characterize the atomic beam we need to understand the divergence of the beam after collimation, as well as the beam width, beam profile and flux at a specified operating temperature. After knowing the solid angle of the atomic beam, the goal is to align it with respect to the Zeeman slower. To do this, we illuminate the atomic beam with a counter propagating laser to probe the D2 cooling transition in ^{133}Cs ($6^2S_{1/2} \rightarrow 6^2P_{3/2}$, $F = 3 \rightarrow F' = 4$, 852 nm detuned by $\Delta = -93$ MHz [19,20], see appendix C). See appendix D for information on Zeeman slowing and our calculations.

The temperature of the ^{133}Cs oven is critical because it directly affects the velocity, the flux and the divergence of the beam after collimation. The normal operating temperature for the ^{133}Cs ample is between 60 °C and 90 °C, which corresponds to a vapor pressure in the oven of 10^{-5} to 10^{-4} torr. Atoms that are not collimated either collide with the walls or with the graphite bank, sticking to them, reducing the background vapor pressure to predicted values around 10^{-9} torr.

We characterize the atomic beam by Doppler-free absorption spectroscopy to determine the atomic flux, width, divergence and average velocity of the beam. To do this we use a laser tuned to the ^{133}Cs D1 transition, 895 nm; despite the D1 line giving a weaker signal as compared to the D2 line, we can still resolve the atoms[1]. We use the crossed beam method,

1. The laser we use is probably not exactly on the cycling transition. Only $\frac{9}{16}$ of the atoms are in $F = 4$, with the other $\frac{7}{16}$ populating $F = 3$; our laser only addresses half the atoms.

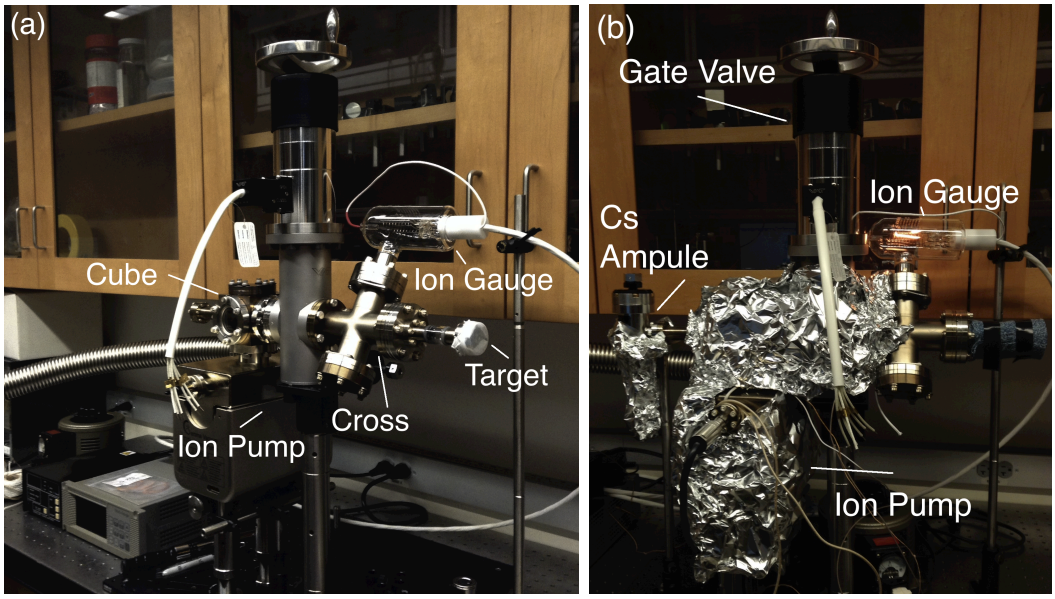

Figure 4.1: Oven test scaffold and final bake. (a) The oven assembly before the addition of the ^{133}Cs ampule. The ^{133}Cs target takes the form of a custom nipple that has a metal-glass-metal transition as a neck. One end of this nipple goes to a reducer and the other to a window, upon which ^{133}Cs impacts. This device is connected to a four-way cross that contains a blank, our Varian 571 ion gauge and the connection to the gate valve. All graphite is contained within the cube and can be easily observed through the windows. (b) The oven in the final bake stage at 170 to 180 °C for two weeks. The ^{133}Cs ampule is attached to the nipple, but will remain cold for the duration of the bake.

where the laser beam is perpendicular to the axis of propagation of the atomic beam, to promote the atoms to an excited state and measure their spontaneous emission [22]. These measurements are performed through the windows of the cube, see Fig. 4.1. For a review of the ^{133}Cs ground state along with the D1 and D2 hyperfine structure, see Steck [18] and appendix C.

In our experiments, Doppler broadening is the dominant contribution to observed line widths in atomic spectra. Doppler-free laser spectroscopy can give high resolution on par with a Fabry-Perot étalon; this is required for us because our narrow atomic beam in combination with its low density produce a weak signal. A standard setup to perform Doppler-free spectroscopy is depicted in Fig. 4.2. We tune the laser frequency to the ^{133}Cs D1 transition using as a reference a probe beam exciting the atoms in a ^{133}Cs vapor cell. We do not need a

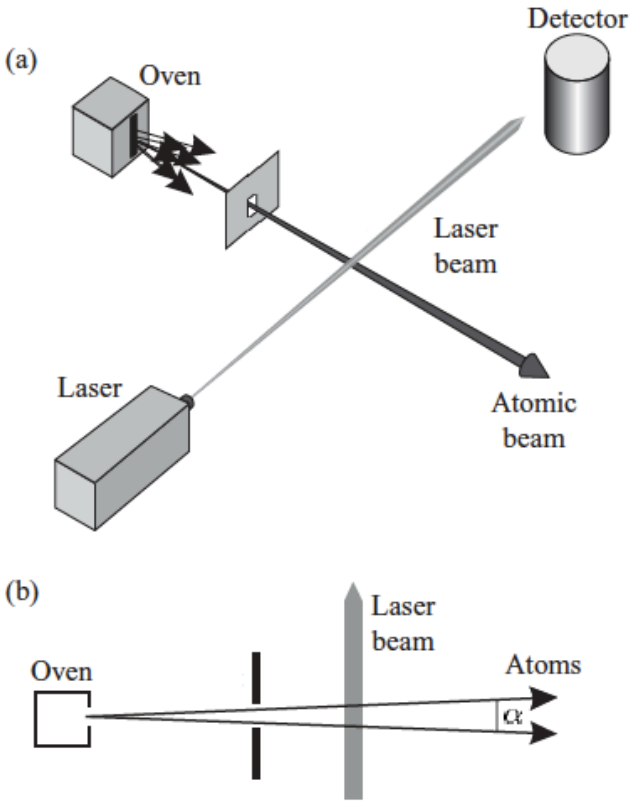

Figure 4.2: Crossed beam doppler-free unsaturated absorption spectroscopy. (a) We perform atomic absorption spectroscopy at the D1 transition. By aiming an 895 nm laser is produced by a laser perpendicular to the direction of the atomic beam. Opposite to the laser is a biased photodetector, with the output sent to an oscilloscope. (b) The atomic velocity component along the laser beam has a small spread of αv_{beam}, where α is the angle of emergence. The diagram is modified from Foot [22] to reflect our set up. See appendix E for more information.

locking circuit for this application due to the stability of the laser. We monitor the frequency through an oscilloscope and notice no significant variation over a few hours, the timescale of taking measurements from the oven.

In our setup we use a beamsplitter to create a pair of beams: one goes through a ^{133}Cs vapor cell and into a biased photodiode where we can observe the absorption lines via oscilloscope, see appendix E. This serves two purposes by allowing us to set and monitor the laser on the transition we want and by allowing us to compare our oven signal to a relatively high pressure vapor cell to confirm our signal. The second beam is sent through a fiber

optic to the oven assembly. The laser is modulated by a sweep frequency of 50 Hz with an amplitude of 0.01 V; this allows us to resolve the absorption features. The laser intensity is held constant at 1.009 mW, below the saturation intensity 2.09 mW [18]; if the laser were saturating the atoms, the signal would be significantly smaller. When the beam is saturated, the atoms cycle between half of the population in the ground state and half in the excited state. The laser, an ECDL (external cavity diode laser), is unstable at low intensity in that power fluctuations increase at lower intensities; its frequency is relatively unaffected. It is critical to keep the laser beam size significantly smaller than the atomic beam otherwise the measurement would reflect the laser beam width instead of the atomic beam width. In this case, the focus of the laser beam is located approximately on the atomic beam.

A translation stage spanning the windows on the cube allow for the collinear movement of the laser source (coupled to an optical fiber) and the detector (photodiode). This allows us to intersect the atomic beam at different points along its propagation axis, and at different heights. With this we performed crossed beam Doppler-free spectroscopy by keeping the horizontal position centered with respect to the window in the cube and varying the vertical position of the translation stage. This allowed us to detect the absorption as a function of the vertical position. The oven ampule was operated at a constant temperature of 91.1 °C while the valve was kept at 143.7°C.

We record the absorption signal directly from the oscilloscope, see Fig. 4.3. The spectral line shape is described by the Cauchy-Lorentz distribution. Line shapes are determined by Doppler, collision and proximity broadening. For atoms, the main effects are collision and Doppler broadening. The spectral line shape observed in the form of absorption dips is relatively sharp because the inner electron energies are not very sensitive to the atom's environment; this is why common absorption spectra for atoms are Lorentzian [21]. Observed spectral line shape and line width are affected by instruments. The observed line shape is a convolution of the intrinsic line shape with the instrument transfer function. This is why

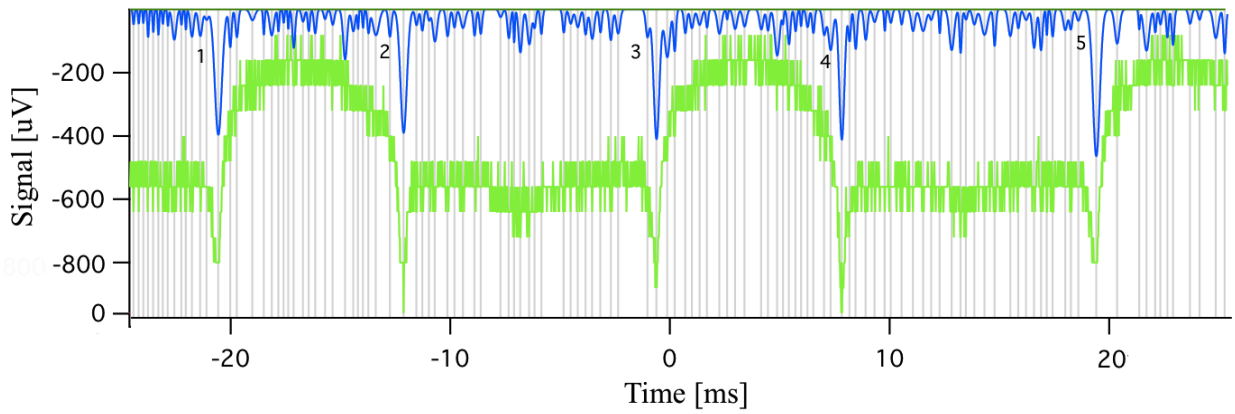

Figure 4.3: Transmission spectrum near the $6^2S_{1/2} \rightarrow 6^2P_{3/2}$ D1 transition. Signal from the detector, see Fig. 4.2, is shown when the laser intersects the atomic beam and scans over the D1 atomic transition. Each dip, labelled 1-5, is an individual measurement, located on the rise and fall of each frequency sweep. The blue overlay is the data after removing the background. The vertical grey lines define the location of the dip minimum.

we elect to use a biased photodiode.

Each data point was taken at a specified height of the photodiode, where each of the 2500 data points taken was an average of 16. Each of these measurements, at a specific height, contains 2.5 sweeps, allowing for 5 absorption dips per height measurement. The amplitude of the dips was determined by curve fitting, see Fig. 4.3. The collected amplitude data as a function of the vertical position of the translation stage allowed us to construct the beam profile of the collimated ^{133}Cs gas, see Fig. 4.4.

4.2 Determination of the Dispersion

The angle of emergence $(\alpha)_{1/e}$, which characterizes the dispersion, is predicted by using ballistic trajectories,

$$\tan(\alpha) = \frac{W_0}{\delta_0} \approx 3^\circ, \tag{4.1}$$

where W_0 is half of the beam width and δ_0 is the is the distance from the center of the collimator to the center of the chamber. This is an overestimate because the atoms are not in a

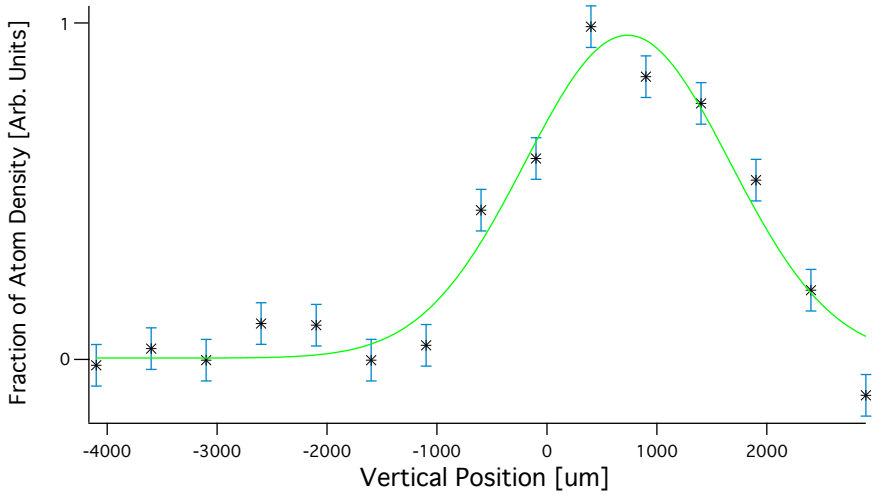

Figure 4.4: Atomic beam profile of a ^{133}Cs gas through a bright-wall collimator. Measured 8.3 cm away from the second collimator, at the center of the window in the cube, the beam is Gaussian to good approximation. The $1/e$ radius of the atomic beam, $d = 1.318 \pm .127$ mm, where the $1/e$ radius is determined by the fit.

regime hot enough to be ballistic in the near field; only in the far field extrapolation do atoms average out to become ballistic at intermediate temperatures. Based on our measurement of the width, we obtain

$$\tan(\alpha)_{1/e} = \frac{1/e \text{ width}}{\delta} \rightarrow (\alpha)_{1/e} = 1.7^{\circ} \tag{4.2}$$

where the ends of the beam are defined by the $1/e$ radius of the beam and $\delta \approx 86$ mm is the distance between the center of the nipple and the point where the laser crosses the atomic beam. This approximation puts the majority of the atoms passing through a third of the predicted angle. Atoms were detected in a spread about 1.4° wide, on each side of the center of the beam, however, but the signal was incredibly weak.

4.3 Determining the Average Velocity and the Atomic Flux

The average velocity of the atomic beam is needed to optimize the Zeeman slower. This velocity is around 240 m/s at 90 °C, see appendix E and Fig. 4.5. An accurate way to experimentally determine the initial velocity at the oven, see Fig. 4.6, is to measure the

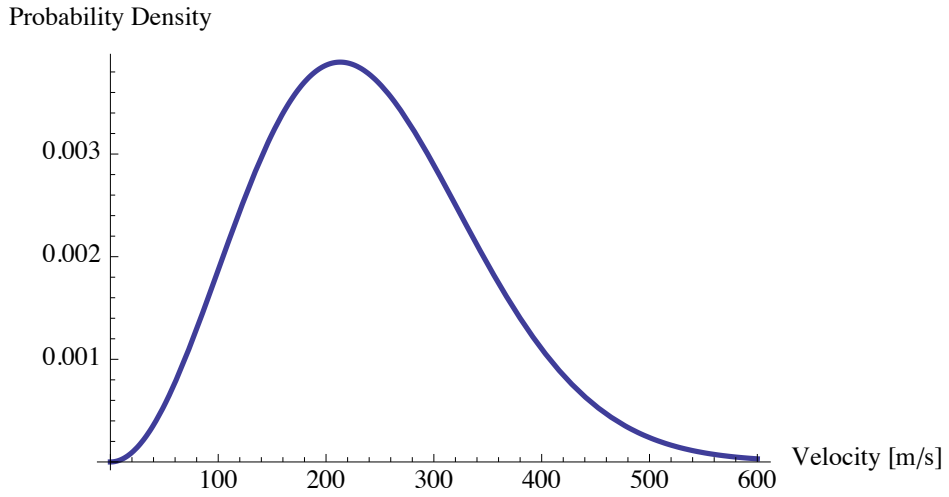

Figure 4.5: Calculated velocity distribution at 90 °C. The velocity distribution according to $f(v) = 4\pi\left(\frac{m}{2\pi k_B T}\right)^{\frac{3}{2}} v^2 \exp\left(\frac{-mv^2}{2k_B T}\right)$, for $T = 90$ °C, where the mean velocity is given by Eq. 2.4.

velocity of the beam at the end of the Zeeman slower. With the final value of the velocity, the initial velocity can be calculated from

$$\bar{v}_f = \sqrt{\bar{v}_i^2 - 2a_z L}, \tag{4.3}$$

where $\bar{v}_f$ is the measured mean final velocity, $\bar{v}_i$ is the initial mean velocity of the atoms leaving the oven, L is the distance over which the atoms were slowed and $a_z = \frac{\eta_s \hbar \Gamma}{2\lambda m}$ is the deceleration, where $\Gamma = 2\pi \times 5$ MHz is the transition line-width for $\lambda = 852$ nm, m is the ^{133}Cs atomic mass and η_s is a safety factor (some factor less than one, parametrizing the ratio between the actual photon scattering rate and the ideal value of $\Gamma/2$).

To determine the number of atoms per unit time that enter the Zeeman slower and that can be captured by the MOT, we need to characterize the atomic flux. We can estimate the flux passing through the second aperture from the first aperture using Eq. 2.13 at the position of the probe laser given that we have measurements of I and I_0. We estimate j, the

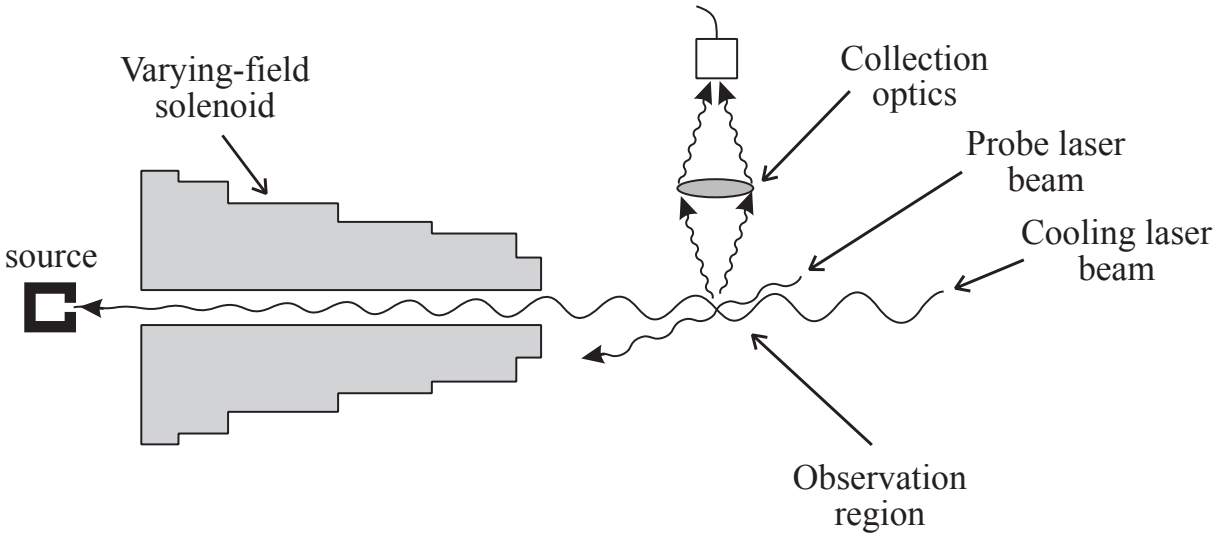

Figure 4.6: Schematic for the measurement of atomic flux. At the end of the Zeeman slower, the flux out of the tube can be measured well before turning on the MOT. Adapted from Foot [22].

light-atom interaction length, as $j \approx 131.8\ \mu$m. The total flux, using Eq. 2.13, is

$$\Theta_{\text{tot},F=4} = \frac{25}{28}\frac{\pi}{\lambda^2 j}\left(\frac{Aa^2}{4\pi}\right)\ln\left(\frac{I_0}{I}\right)\sqrt{\frac{2k_B T}{\pi m_{(\text{Cs})}}} = 4.57\times 10^9\ \frac{\text{atoms}}{\text{s}}, \tag{4.4}$$

where $T = 90\ ^\circ$C and the area of the aperture A is substituted for $\frac{Aa^2}{4\pi}$, where a is the length of the collimator, (see Fig. 2.2), to account for the flux traveling through two apertures. The second aperture area is small compared to the separation between the two apertures. The total atomic flux reaching the cube is $\frac{16}{9}$ multiplied by Eq. 4.4,

$$\Theta_{\text{tot}} = 8.14\times 10^9\ \frac{\text{atoms}}{\text{s}} \tag{4.5}$$

This atomic flux is sufficient to keep MOT loading time around two seconds given that the capture rate of our MOT will be between 15-20%. Our measured flux is about 30% of the

predicted flux obtained from Eq. 2.7,

$$\Theta_{0,\text{tot}} = 1.53 \times 10^{10} \ \frac{\text{atoms}}{\text{s}}. \tag{4.6}$$

Ideally, we would expect to observe about 56% ($\frac{9}{16}$) of the predicted flux. This discrepancy is rooted in (i) how the atoms coat the apertures and the walls of the collimation nipple at room temperature, preventing some reemission, and (ii) our imaging scheme. The nipple walls and apertures were at room temperature, meaning that if Cs atoms impacted upon them, the atoms were more likely to stick. In typical operation, the apertures are heated and the nipple is cooled to prevent reemission from the walls; we expect to see higher flux when the apertures are heated despite the coldfinger cooling the nipple walls to prevent reemission.

The imaging laser was our main problem in determining the flux more accurately. The laser beam was not on a cycling transition and it only addressed the $F = 4$ total atomic angular momentum state; only $\frac{9}{16}$ of the atoms were in the $F = 4$ state while the other $\frac{7}{16}$ were in the $F = 3$ state[2]. Our measured value of the flux is comparable to the values reported at the end of the Zeeman slower in a similar oven setup, $8 \times 10^8 \ \frac{\text{atoms}}{\text{s}}$, [19, 20]; these reported values are at lower temperatures (60-80 °C) and take into account that about 15% of the flux is trappable by the MOT.

Given the flux of this experiment is two orders of magnitude below that of Bashkar *et al* [11], the graphite banks in our setup could withstand greater than ≈ 750 hours of direct atomic beam bombardment before the sticking coefficient could be expected to drop below $\gamma = .4$. None of the graphite banks are in the way of the beam; at most they would receive $\frac{1}{3}$ of the flux from the oven, extending their lifetime to over ≈ 2250 hours of operating time at 90 °C before dropping below $\gamma = .4$. The graphite pieces can be partially restored through the outgassing of captured Cs; by heating the vacuum elements that the graphite banks

2. Cs atomic ground states are evenly distributed between the hyperfine splitting in the $F = 3$ state (7 ground states) and $F = 4$ (9 ground states) state.

are suspended from, the banks can be emptied of graphite over time. We use around 5 g of graphite in the construction of the oven; while about the same weight as the Cs, the majority of Cs will go to the ion pumps, the walls and the experiment.

This effusive oven can be readily compared and contrasted with other contemporary designs like that in Tino *et al* [23]. Our design can be easily modified for all commonly used alkali and alkaline earth metals, as well as a number of lanthanides.

CHAPTER 5

CONCLUSION

In conclusion, an effusive oven for ^{133}Cs was created for an ultracold atom experiment. Using a bright-wall collimation scheme combined with a highly efficient coldfinger, a well collimated atomic beam was created. To characterize the beam, we reported the width of the atomic beam, $1.318 \pm .127$ mm, the divergence, $\alpha_{1/e} = 1.7^{\circ}$, and the flux passing through the second aperture from the first aperture at 90 °C, $\Theta_{\text{tot}} = 8.14 \times 10^9 \ \frac{\text{atoms}}{\text{s}}$; we also predicted the mean velocity at 90 °C, 240 m/s.

The atomic flux is comparable to what we obtain from a similar Cs oven system operating in our laboratory [19,20]. The $1/e$ radius criterion of the atomic beam width gives us a value smaller than the apertures; these are the atoms that are most likely to end up being caught by the MOT. Atoms were detected in a spread about 1.4° wide, on each side of the center of the beam. Our measurement was near the collimator, which put our measurement in the near field. The measurement location in the near field and using the $1/e$ radius also accounts for the small divergence.

The oven functions within our expectations and produces results that we can explain. The next step will involve the construction of the Zeeman slower and the addition of oven/Zeeman slower system to the main experiment.

CHAPTER 6

OUTLOOK

The ^{133}Cs effusive oven project, while originally intended to replace the aging ^{133}Cs oven in Prof. Cheng Chin's ^{133}Cs experiment, will be used for his new mixture experiment. The Cs oven in the ^{133}Cs experiment has stabilized in pressure due to some external improvements since this project was started, freeing up this device. The mixture species is currently speculative. The question of whether we are going to use bosonic or fermionic potassium is still open. We may use ^{39}K or ^{40}K (boson, fermion respectively). At this time, it is slated for use in Prof. Chin's new proposed ^{133}Cs-potassium (CsK) quantum gas microscope mixture experiment. The plan is to use two separate atomic ovens for ^{133}Cs and K, which means a separate Zeeman slower and separate MOTs. This will allow the CsK team to bypass problems associated with dual-species ovens. The Cs Zeeman slower will be completed by another student in the NSF Physics REU.

There are some minor modifications to be made to this device, notably the addition of a third graphite collimator to ensure that the edges of the beam do not impact upon the inside of Zeeman slower tube and so that the loading diameter of the beam is smaller than the size of our intended MOT beams. These will be added to the system in the next leg of the project before the addition of the Zeeman slower. The oven is the first of many systems to be created for the proposed KCs experiment. The role of the effusive oven in the partially assembled system can be seen in Fig. 6.1.

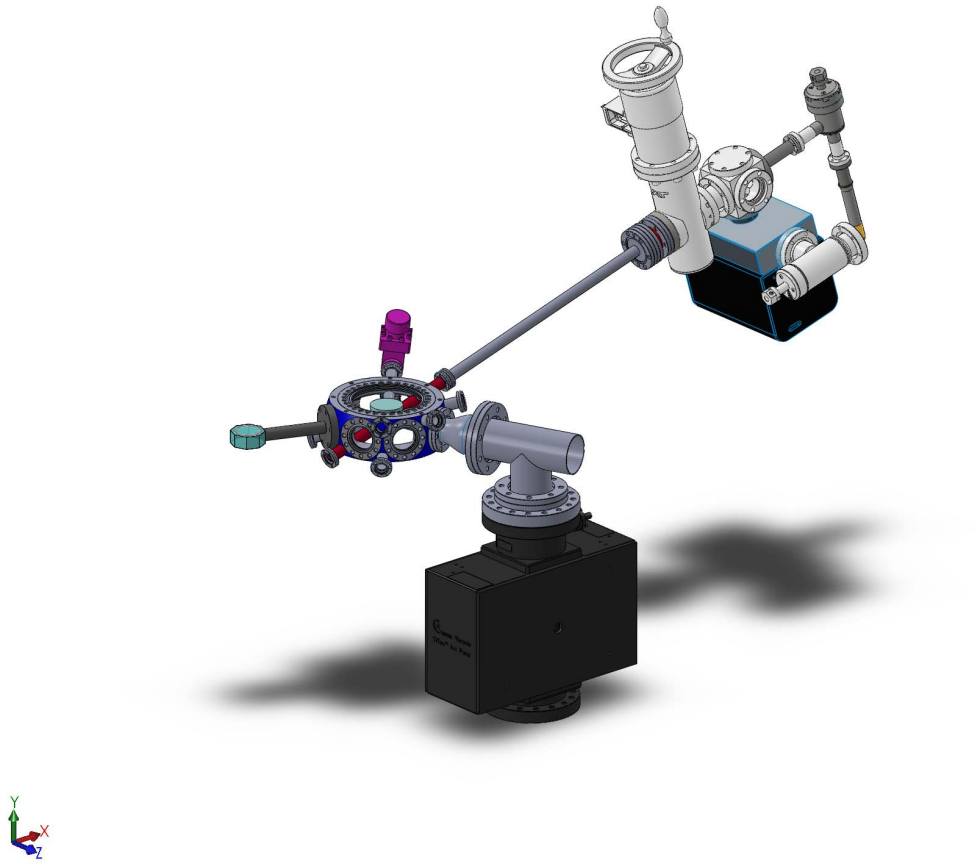

Figure 6.1: Quantum gas microscope experiment layout. The final experiment will contain a high resolution optical microscope over the glass cell, as well as a pair of Chin Lab Bitter Electromagnets [24]. The oven is mounted at an angle of 22.5° in the XZ plane and 13° in the XY plane.

Part II

Appendices and Supplemental Information

APPENDIX A

TABLE OF VACUUM COMPONENTS

We have neglected to include information relating to screws, regular gaskets and other miscellaneous parts. Prices in USD.

Item	Supplier, Part Number	Quantity, Price
^{133}Cs	Sigma-Aldrich, 239240-5G	1, $320.00
^{133}Cs Glass Receptacle	MDC, Custom	1, $150.00
All-Metal Valve for ^{133}Cs	MDC, MAV-075-V	1, $805.00
All-Metal Valve for Ion Pump	MDC, MAV-150-V	1, $645.00
Ion Pump	Gamma Vacuum, 45S-CV-2D-SC-N-N	1, $2100.00
Cube	CU150-6	1, $871.00
Reducers	275X133	2, $73.00
Windows	1001401	2, $259.00
Gate Valve	VAT, 48132-CE05	1, $7880.00
Nipple	Kurt J. Lesker, Custom	1, $139.40

APPENDIX B

COLDFINGER DESIGN

This design was compiled using an educational license for Autodesk Inventor®. It appears in full below. Note that the water cooling connections are not in the drawing. They attach to the top and bottom copper rectangular prisms. The location of water cooling loops in the copper and how to make them is up to interpretation. We made three holes to make a U-shaped water loop after plugging one of the holes; swage-lock connectors to plastic tubing bring water from the laboratory supply at 3.8 liters/minute. All measurements in inches.

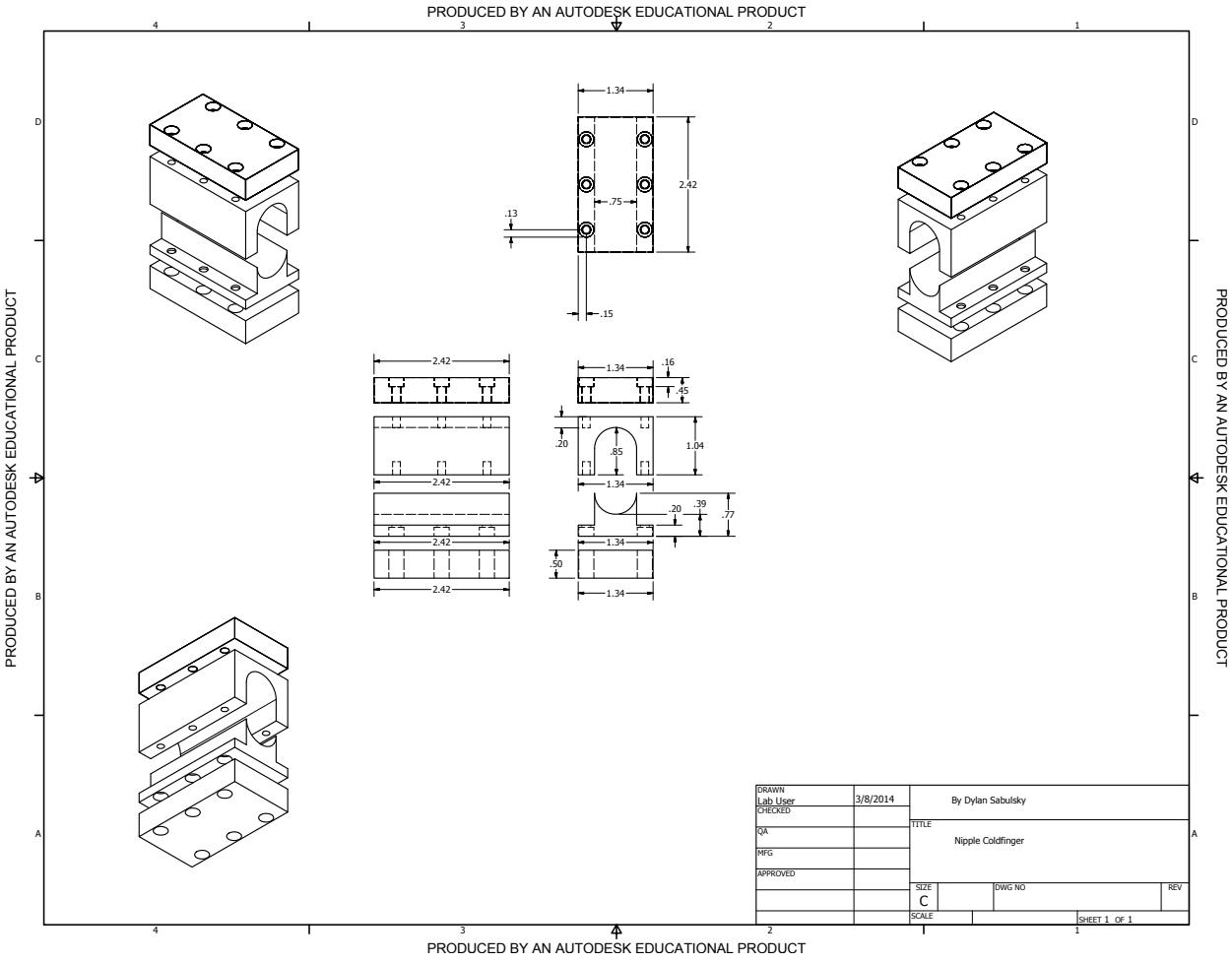

Figure B.1: Coldfinger design.

APPENDIX C

VAPOR PRESSURE AND HYPERFINE STRUCTURE OF ^{133}CS

The diagrams below were adapted from Steck [18], see the manuscript for details. The vapor pressure model is derived from the following:

$$\log_{10}(P_v) = -219 + \frac{1089}{T} - .08T + 95\log_{10}(T) \text{ (Solid Phase) and} \tag{C.1}$$

$$\log_{10}(P_v) = 8 - \frac{4006}{T} - .0006T - .2\log_{10}(T) \text{ (Liquid Phase)} \tag{C.2}$$

where T is temperature in Kelvin and P_v is the vapor pressure in torr.

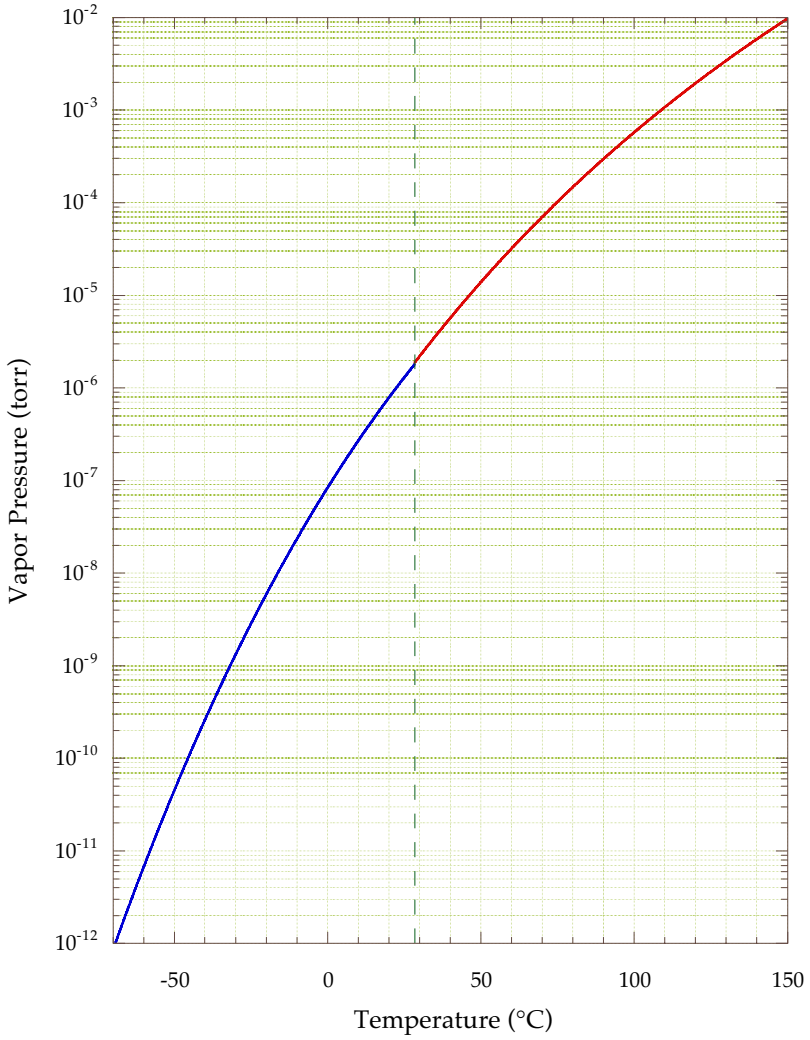

Figure C.1: ^{133}Cs vapor pressure. The vertical line indicates the melting point, 28.55 °C.

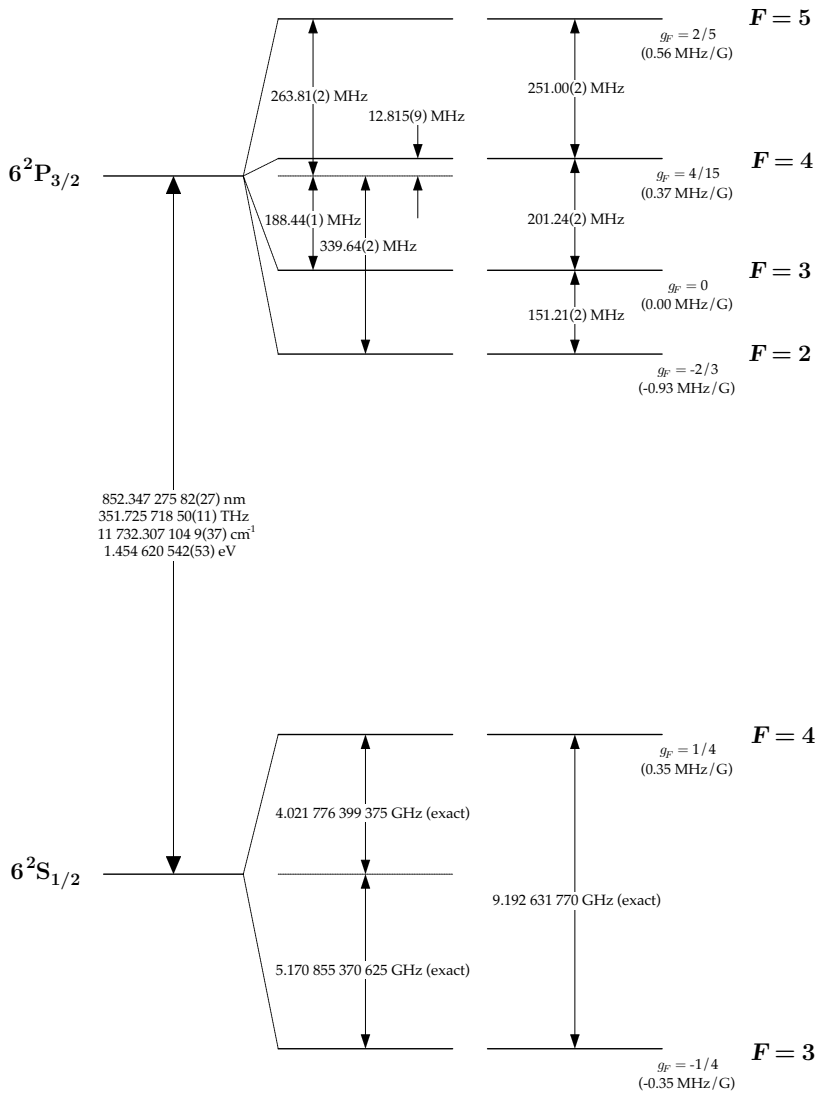

Figure C.2: ^{133}Cs D2 hyperfine structure. Corresponding Zeeman splittings are shown.

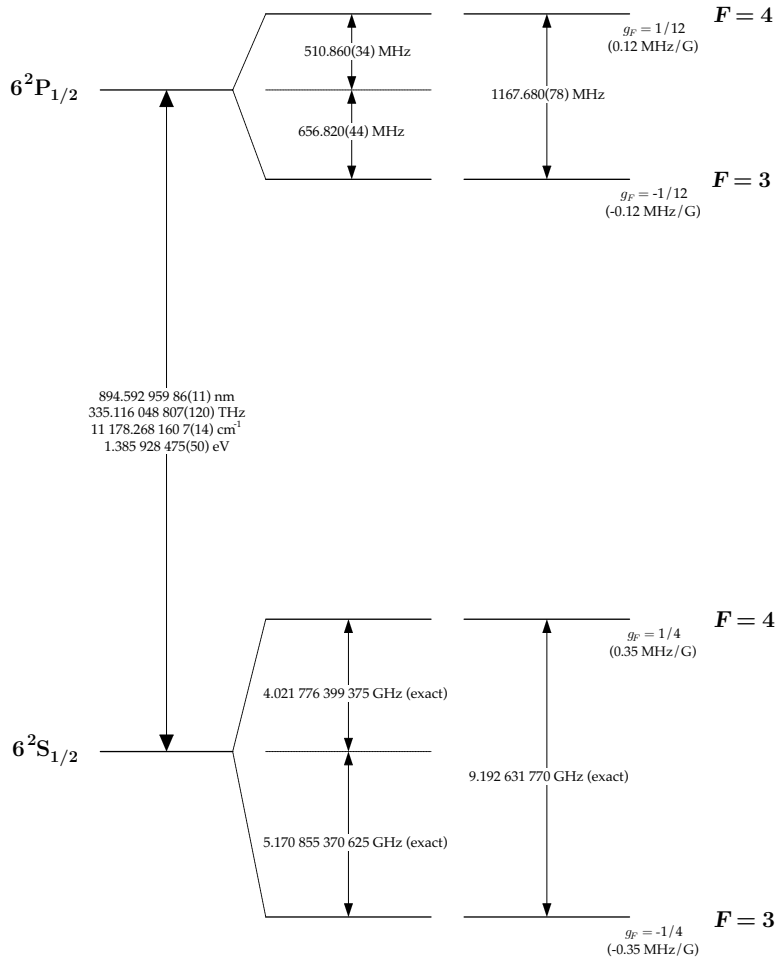

Figure C.3: ^{133}Cs D1 hyperfine structure. Corresponding Zeeman splittings are shown.

APPENDIX D

ZEEMAN SLOWERS AND CALCULATIONS

The ingenious method in which an atomic beam traveling down the axis of a tapered solenoid is slowed down takes advantage of the Zeeman effect. The Zeeman effect of the varying magnetic field perturbs the atomic energy levels such that the transition frequency matches a constant laser frequency. For constant deceleration from some initial velocity v_0 at $z = 0$, we know that the velocity as a function of distance is

$$v_0^2 - v^2 = 2az. \tag{D.1}$$

To ensure that no atoms are left behind, the deceleration is usually half of the maximum value, $a = a_{\max}/2$. The stopping distance is defined as

$$L_0 = \frac{v_0^2}{a_{\max}}. \tag{D.2}$$

During constant deceleration, the velocity at some distance from the starting point is given by

$$v = v_0\left(1 - \frac{z}{L_0}\right)^{\frac{1}{2}}. \tag{D.3}$$

The frequency shift caused by the Zeeman effect needs to obey the following criterion in order to compensate for the Doppler shift as the atoms slow down:

$$\omega_0 + \frac{\mu_B B(z)}{\hbar} = \omega + kv. \tag{D.4}$$

The Zeeman shift of an atomic magnetic moment μ_B only increases the atomic resonance frequency from ω_0, the resonance frequency at zero field. The Doppler shift adds to the laser

frequency ω. The required magnetic field profile is

$$B(z) = B_0\left(1 - \frac{z}{L_0}\right)^{\frac{1}{2}} + B_{\text{bias}} \tag{D.5}$$

from $0 \leq z \leq L_0$ where $B_0 = \frac{\hbar v_0}{\lambda \mu_B}$. The condition for the average velocity of the atoms to be centered on zero ie bringing the atoms to a complete stop at the end of the tapered solenoid is $\mu_B B_{\text{bias}} = \hbar\omega - \hbar\omega_0$. It is more common to leave the atoms with a small velocity to travel to the MOT, where they are captured [22].

The following Mathematica calculations we made in preparation for an NSF Physics REU project in Prof. Chin's group, made to follow the oven project. The goal is to make a combined source and Zeeman slower to attach to our main chamber to load ^{133}Cs at velocities that our magneto-optical trap can capture. It is the next step after the ^{133}Cs oven; a ^{133}Cs Zeeman slower, to slow the atoms down from ≈ 240 m/s to less than ≈ 30 m/s in about 61 cm, given the assumptions below. After consultation, a length of 40 cm was confirmed.

```
(*Zeeman Slower Calculations for Cs-133 in the KCS Quantum Gas Microscope Experiment.
   By Paloma, Dylan and Logan*)

vf = 20(*final velocity, m*); m = 2.2077*10^-25(*mass of cs atom, kg*); n = 0.8
(*safety factor*); Γ = 2*Pi*5*10^6(*scattering rate*); h = 6.626*10^-34
(*planck's constant*); λ = 852*10^-9(*wavelength, m*); a = -(n*(Γ/(2*Pi))*h)/(2*λ*m)
(*acceleration, m/s*); k = 1.38*10^-23(*boltzmann constant*); T = 353.0
(*temperature in kelvin*); μ0 = 4π*10^-7; v0[L_] := Sqrt[(vf)^2 + 2*a*L];
F[v0_] := Sqrt[2*m/(Pi*k*T)]*Exp[(-m*v0^2)/(2*k*T)](*distribution with modified normalization factor*);
Integrate[F[v0], {v0, 0., 210.}](*???*); G = Integrate[F[v0], {v0, 0, b}]
(*velocity fraction*); b = Sqrt[(vf)^2 - 2*a*L](*b is initial velocity*);
captureSize = 0.01016(*radius of our loading angle in meters *);
divergenceAngle = .94*Pi/180(* assumes 1.88 degree divergence,
3mm aperture at the cube with graphite collimator*);
AngleFrac = Min[1, captureSize/(L*divergenceAngle)];
```

```
(*Velocity capture fraction as a function of the Zeeman Slower Length*)
Plot[{G, If[0 < L < .619, 0]}, {L, 0, 2}, PlotStyle → Thick,
 AxesLabel → {"Zeeman Slower Length", "Atom velocity capture fraction"},
 PlotRange → {0, 1}, Filling → {1 → {2}}]
(*Shaded area is our velocity selection for a 3mm aperture in the graphite at
 the cube*)
```

Atom velocity capture fraction

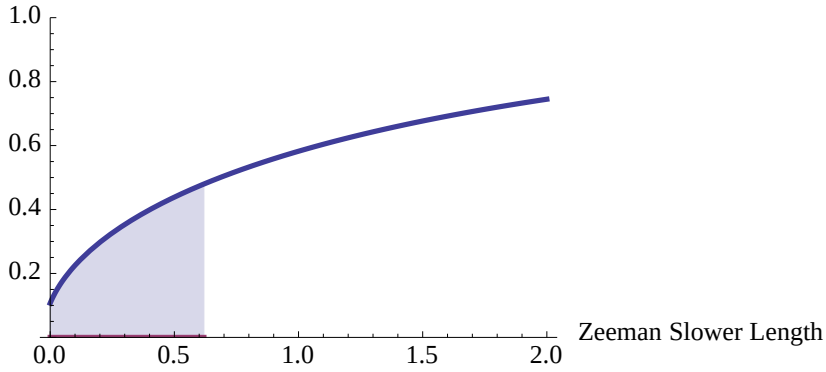


```
Plot[{G * AngleFrac, If[0 < L < .619, 0]}, {L, 0, 3}, PlotStyle → Thick,
 AxesLabel → {"Zeeman Slower Length",
   "Atom velocity capture fraction times Angular capture fraction"}, PlotRange → {0, .8},
 Filling → {1 → {2}}]
(*that shade tho*)
```

Atom velocity capture fraction times Angular capture fraction

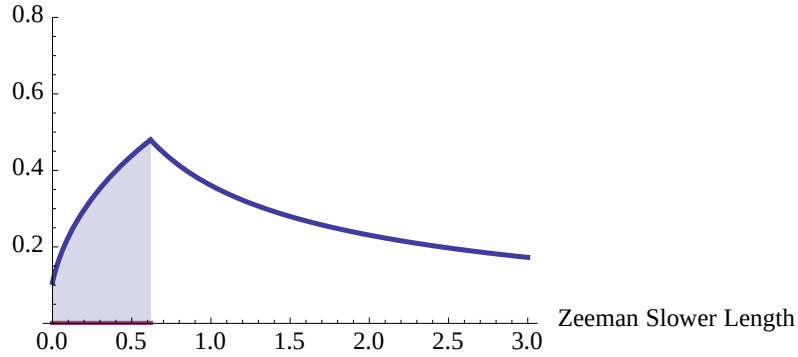

$$\text{Leng} = \frac{\text{captureSize}}{\text{Tan[divergenceAngle]}}$$ (*length of zeeman slower in meters*)

```
0.619226
```

APPENDIX E

CROSSED BEAM DOPPLER-FREE ABSORPTION SPECTROSCOPY

The angular frequency of radiation in the laboratory frame, ω, and the angular frequency seen in a moving reference frame, ω' in some frame $\mathbf{v}$, is shown to be

$$\omega' = \omega - kv, \tag{E.1}$$

where the wavevector has a magnitude $k = \omega/c = 2\pi/\lambda$. It is the component of the velocity along $\mathbf{k}$ that leads to the Doppler effect [22]. We consider the Doppler effect on the absorption of a gas where each atom absorbs radiation at some frequency ω_0 in the rest frame when $\omega' = \omega_0^2$. Atoms moving with some velocity v absorb radiation with the criterion $\delta = \omega - \omega_0 = kv$ or equivalently,

$$\frac{\delta}{\omega_0} = \frac{v}{c}. \tag{E.2}$$

The fraction of atoms with velocity in the range v to $v + \mathrm{d}v$ is

$$f(v)dv = \sqrt{\frac{M}{2\pi k_B T}} \exp\left(-\frac{Mv^2}{2k_B T}\right) dv \tag{E.3}$$

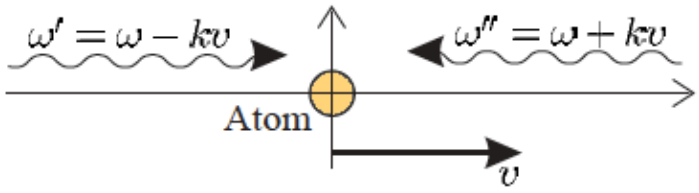

Figure E.1: The observed frequency of radiation and the doppler effect. Adapted from Foot [22].

where the most probable speed for atoms of mass M at temperature T is $\tilde{v} = \sqrt{2k_BT/M}$. The absorption has the Gaussian line shape function

$$g_D(\omega) = \frac{c}{\tilde{v}\omega_0\sqrt{\pi}} \exp\left\{ -\frac{c^2}{\tilde{v}^2}\left(\frac{\omega-\omega_0}{\omega_0}\right)^2\right\}. \tag{E.4}$$

The maximum value occurs when $\omega = \omega_0$ and the function is at the $1/e$ radius at $\omega - \omega_0 = \delta_{1/2}$ where

$$\ln(2) = \left(\frac{c\delta_{1/2}}{\tilde{v}\omega_0}\right)^2. \tag{E.5}$$

One way of logging the velocity of atoms with doppler broadened lines is to use the full width at half maximum when $\Delta\omega_D = 2\delta_{1/2}$ is given as

$$\frac{\Delta\omega_D}{\omega_0} = 2\sqrt{\ln(2)}\frac{\tilde{v}}{v}. \tag{E.6}$$

Kinetic Theory gives the most probably speed in a gas; in a gas with a Maxwellian distribution of velocities in an effusive atomic beam, the distribution is

$$f(v) = v^3 \exp\{-v^2/\tilde{v}^2\}, \tag{E.7}$$

where the most probable speed is $\sqrt{3/2}\tilde{v}$ and the room-mean-square velocity is $\sqrt{2}\tilde{v}$[1]. the extra factor of v for a beam arises from the way atoms effuse through a sufficiently small hole of some area A. Atoms are incident on the surface of A at a rate $N(v)\ vA/4$ where $N(v)$ is the number density of atoms. Faster atoms are more likely to pass through the hole. Integration over v gives the kinetic theory result that $N\bar{v}A/4$ for the flux arriving at the surface of A; N is now the total number density. The value for the mean speed $\bar{v}$ is bounded

1. We can distinguish between two components of the velocity distribution: (i) a longitudinal distribution with velocities $v_z(T)$ and (ii) a transverse distribution with velocities $v_{xy}(T, f)$. The longitudinal distribution is determined by the temperature T of the source while the transversal distribution fulfills the boundary conditions of the apertures and is determined by the collimation ratio f.

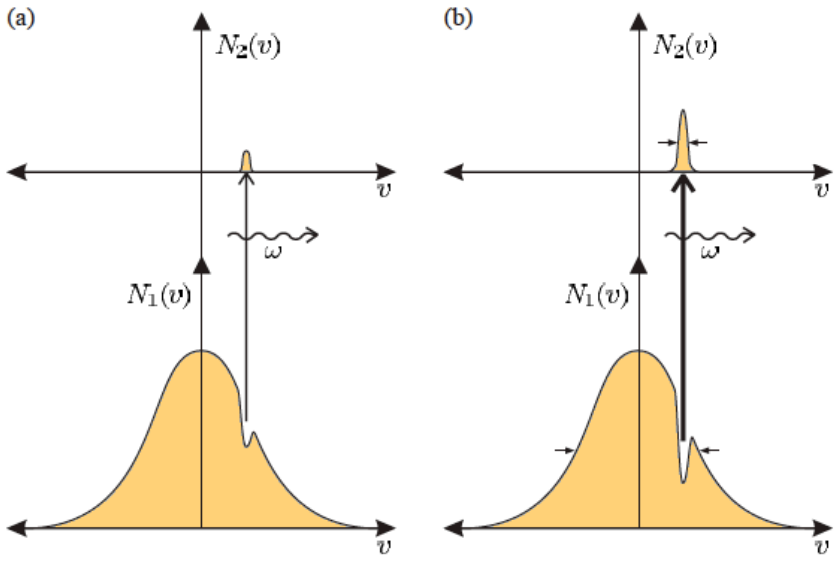

Figure E.2: Saturated absorption. (a) While a weak beam does not significantly alter the number density of atoms in each level, a signal can still be seen in our set up. (b) A high-intensity laser beam burns a hole in the distribution. Note this is a gaussian form while considering wavevector versus number density. This is not ideal for our situation; we do not have a high density of atoms. This, coupled with us using a suboptimal transition (D1 instead of D2) and the limitations of our photodiode lead us to use a beam slightly below saturation; we receive the best signal there. The signal deteriorates rapidly at the saturation intensity. One can also see the inhomogeneity of Doppler broadening if the translation stage is not parallel to the beam. Adapted from Foot [22].

by the most probable velocity $\tilde{v}$ and the root-mean-square velocity $\sqrt{2}\tilde{v}$.

The Doppler effect on the absorption of a gas is an inhomogeneous broadening mechanism in that each atom interacts with the radiation differently due to their velocity and the frequency detuning. Absorption and emission then depend on the velocity of each atom. In our experiment, we use a simple set up to make sure our D1 laser stays at the right frequency. See below.

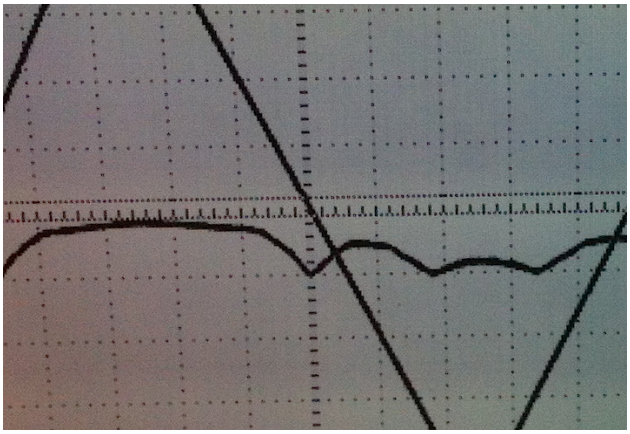

Figure E.3: Oscilloscope readout of the sweep frequency and laser sitting on resonance. The large triangular wave is our sweep frequency, 50 Hz at an amplitude of .01 V, and the dip center just below zero is the D1 transition at $\approx$ 895 nm. We leave the laser on this transition without any active locking device.

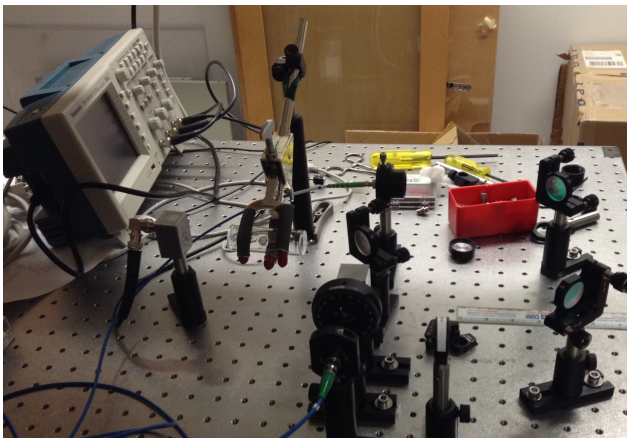

Figure E.4: Optical setup for monitoring laser frequency stability. The laser comes in through the angle-cut fiber optic at the bottom, through the cube where it splits into the ^{133}Cs cell/photodiode leg and the two mirrors which direct the beam into the angle cut fiber optic in the middle of the photo. This second fiber goes to the experiment.

REFERENCES

[1] X. Zhang, C. L. Hung, S. K. Tung, N. Gemelke and C. Chin. *New Journal of Physics* **13**, 045011 (2011).

[2] C. L. Hung, X. Zhang, N. Gemelke and C. Chin. *Nature* **470**, 236-239 (2011).

[3] C. V. Parker, L.C. Ha and C. Chin. *Nature Physics* **9**, 769 (2013).

[4] K. J. Ross and B. Sonntag. *Rev. Sci. Instrum* **66**, 4409 (1995).

[5] J. Schindler, Masters Thesis, University of Innsbruck, 2011.

[6] H. Haken and H. C. Wolf. *Atom- und Quantenphysik*, Springer, 1990.

[7] W. Demtröder, *Laser Spectroscopy: Basic Concepts and Instrumentation*, Springer, 2010.

[8] N. F. Ramsey. *Molecular Beams*, Oxford University Press, 1985.

[9] F. B. Dunning and R. G. Hulet. *Atomic, Molecular, and Optical Physics: Atoms and Molecules*. London: Academic Press, 1996.

[10] H. Pauly. *Atom, Molecule and Cluster Beams I: Basic Theory, Production and Detection of Thermal Energy Beams*. Heidelberg: Springer-Verlag, 2000.

[11] N. D. Bhaskar, C. M. Kahla, R. P. Frueholz, R. A. Cook. *Aerospace Corp*, 1988.

[12] N. F. Ramsey. *Thermal Atom Beams, in Atomic, Molecular and Optical Physics: Atoms and Molecules*, edited by F. B. Dunning and R. G. Hulet, Volume 29B of Experimental Methods in the Physical Sciences, Chapter 1, Academic Press, 1996.

[13] H. J. Metcalf and P. van der Straten. *Laser Cooling and Trapping*, Springer, 1990.

[14] R. P. Frueholz, N. D. Bhaskar, J. C. Camparo, B. Jaduszliwer and C. M. Klimcak. Aerospace Corp, 1986.

[15] M. A. Bouchiat. *J. Phys.* (Paris) **24**, 379 (1963).

[16] S. Wexler. *Rev. Mod. Phys.* **30**,402 (1958).

[17] M. H. Hablanian. *High-Vacuum Technology: A Practical Guide*. New York: Marcel Dekker, 1997.

[18] D. A. Steck, Cesium D Line Data, Los Alamos National Laboratory, 2003.

[19] C.-L. Hung, Ph. D dissertation, University of Chicago, 2011.

[20] X. Zhang, Ph.D dissertation, University of Chicago, 2012.

[21] M. J. Hollas. *Modern Spectroscopy*. West Sussex: Wiley, 1996.

[22] C. J. Foot. *Atomic Physics*. Oxford: Oxford University Press, 2005.

[23] M. Schioppo, N. Poli, M. Prevedelli, St. Falke, Ch. Lisdat, U. Sterr and G. M. Tino. *Rev. Sci. Instrum.* **83**, 103101 (2012).

[24] D. Sabulsky, C.V. Parker, N. Gemelke and C. Chin. *Rev. Sci. Instrum.* **84**, 104706 (2013).